Journal of Catalysis **187,** 321–331 (1999)
Article ID jcat.1999.2606, available online at http://www.idealibrary.com on IDEAL®

Kinetics of the $CO + N_2O$ Reaction over Noble Metals

I. Pt/Al_2O_3

P. Granger,[1] P. Malfoy, P. Esteves, L. Leclercq, and G. Leclercq

Laboratoire de Catalyse, UPRESA 8010, Université des Sciences et Technologies de Lille, Bâtiment C3, 59655 Villeneuve d'Ascq Cédex, France

Received February 3, 1999; revised June 4, 1999; accepted June 20, 1999

The kinetics of the $CO + N_2O$ reaction on Pt/Al_2O_3 have been studied between 260 and 320°C with partial pressures ranging from 1×10^{-3} to 8×10^{-3} atm for N_2O and 4×10^{-3} to 14×10^{-3} atm for CO. A mechanism has been selected from those suggested in the literature. It involves molecular adsorptions of N_2O and CO and a dissociation step of adsorbed N_2O on a nearest neighbor vacant site which is assumed to be rate limiting. A rate expression has been derived which led to the estimation of the rate constant of N_2O dissociation and of the equilibrium adsorption constants of N_2O and CO. Enthalpies of adsorption of N_2O and CO, $\Delta H_{ads,CO}$ and $\Delta H_{ads,N_2O}$, and the energy of activation for adsorbed N_2O dissociation, E, have been estimated in order to model temperature-programmed experiments. A divergence between experimental and calculated conversion vs temperature has been observed mainly at high conversion. Such a discrepancy has been mainly assigned to changes in the adsorption enthalpy of CO and NO with the adsorbate surface coverage. Such an effect has been tentatively quantified. © 1999 Academic Press

1. INTRODUCTION

During the past two decades, the kinetics of the $CO + NO$ reaction, involved in automotive catalytic converters, has been extensively studied, particularly over Rh-based catalysts (1, 2). All these investigations have provided reliable information of practical and fundamental interest. Presently, three-way catalysts (TWC) have a good activity for the $CO + NO$ reaction and the mechanism of this reaction seems well established. But, during the cold start of TWCs (at low temperature and conversion), NO seems to be mainly transformed into N_2O, and the intermediate formation of N_2O and its subsequent reduction by CO is still under concern since the literature reveals some conflicting arguments on the real importance of a two-step reaction pathway involving the intermediate formation of N_2O in the reduction of NO by CO (3, 4).

From an experimental point of view the intermediate formation of N_2O during the $CO + NO$ reaction is observed without any ambiguity below the light-off temperature (5, 6), while only N_2 is observed in the actual operating conditions (100% NO conversion), after the cold start of a three-way catalyst (7–9). In fact, the $CO + N_2O$ subreaction during the reduction of NO by CO has been neglected for a long time probably because a few studies have shown that the rate of the isolated $CO + N_2O$ reaction is substantially lower than that of the $CO + NO$ reaction either on Pt- (10) or on Rh-based catalysts (9). These results could explain why the elementary steps related to the readsorption of N_2O and the transformation of adsorbed N_2O molecules on noble metals have often been omitted in the mechanism for the $CO + NO$ reaction (6, 11–13), until Cho *et al.* (8) found that the reduction of N_2O by CO plays a major role in the $CO + NO$ reaction on Rh/Al_2O_3. Further kinetic investigations of the isolated $CO + N_2O$ and during the $CO + NO$ reaction on Rh at 310°C, above the light-off temperature performed by the same author (14, 15), has supported his previous statements that N_2O is able to readsorb on Rh and react with adsorbed CO. A rate enhancement has been observed for the intermediate $CO + N_2O$ reaction (during the $CO + NO$ reaction) in comparison with that of the isolated reaction. This has been explained by repulsive interactions between N atoms (from the dissociation of NO) and CO molecules in the adsorbed layer which favor the desorption of CO and the subsequent adsorption and decomposition of N_2O formed in the $CO + NO$ reaction. This interpretation led Cho *et al.* to the conclusion that the lack of N_2O observation above 300°C may be due to the fast reaction between N_2O and CO.

In previous work performed in our laboratory dealing with the kinetics of the $CO + NO$ reaction over Pt (16), Rh, and bimetallic Pt–Rh catalysts supported on alumina (17), we have confirmed that N_2O is the major N-containing product on Rh-based catalysts below the light-off temperature. However, the changes in the selectivity for N_2O formation (S_{N_2O}) is very different for Pt/Al_2O_3 on the one hand and Rh and Pt–Rh on alumina on the other hand. As a

[1] To whom correspondence should be addressed. Fax: 33 3 20 43 65 61. E-mail: Pascal.Granger@univ-lille1.fr.

0021-9517/99 $30.00

matter of fact, with Pt/Al_2O_3, first S_{N_2O} decreases continuously and slowly as temperature and conversion increases and then it suddenly decreases at the light-off temperature (50% conversion) and becomes very low above 75% conversion, while on Rh/Al_2O_3 and $Pt–Rh/Al_2O_3$, S_{N_2O} remains almost constant and starts to decrease only for high NO conversion ~80%. This observation seems to suggest that the $CO + N_2O$ reaction occurs more readily on Pt than on Rh. Such a difference in N_2O formation can arise from differences in N_2O and NO adsorption on Pt and on Rh. Hence it would be interesting to measure the adsorption equilibrium constant of N_2O (λ_{N_2O}) in order to compare with λ_{NO} already determined in our previous study (16).

In this first paper we report a detailed kinetic study of the $CO + N_2O$ reaction over Pt/Al_2O_3. In this study, we have selected several mechanisms proposed in the literature and derived the corresponding rate expressions, which have further been compared to our experimental results according to the same procedure as that used for the $CO + NO$ reaction and described in an earlier paper (16). This procedure has shown that only one rate expression is in agreement with the experimental results. Kinetic and thermodynamic constants have been calculated assuming this model.

From the values of these parameters we will discuss the adsorptive and the catalytic properties of Pt in the reduction of NO and N_2O by CO which influence the selectivity of Pt for the formation of N_2O. The temperature dependency of these parameters has also been investigated using graphic and optimization methods. Finally, in the second part of this paper we will try to validate our kinetic model for the $CO + N_2O$ reaction in conditions closer to the cold start of a three-way catalyst.

2. EXPERIMENTAL

The Pt catalyst was prepared by impregnating the support γ-Al_2O_3 (100 $m^2\ g^{-1}$) with a solution of hexachloroplatinic acid to yield 1 wt% Pt. The preparation procedure, including wet impregnation, calcination in air at 450°C, and reduction in flowing H_2 at 500°C, was similar to that described in reference (16). The metal dispersion estimated from hydrogen chemisorption measurements was 0.58, the corresponding average particle size of Pt was ~1.7 nm. The catalyst was in powder form with an average grain diameter of ~80 μm.

The experimental setup was detailed in Refs. (16) and (17). The $CO + N_2O$ reaction was studied in a fixed bed flow reactor at atmospheric pressure under the following experimental conditions: 0.07 to 0.60 g of catalyst mixed with 0.28 to 2.4 g of α-Al_2O_3. The global flow rate was maintained at 10 L h^{-1}, which gave space velocities between 8000 and 70,000 h^{-1}. The initial partial pressures ranged from 1×10^{-3} to 8×10^{-3} atm for N_2O and 4×10^{-3} to 14×10^{-3} atm for CO (1 atm ~10^5 Pa). Prior to the reaction the catalyst samples were preheated in flowing hydrogen (3 L h^{-1}) at 500°C for 7 h and then outgassed in flowing nitrogen at 400°C.

Differential kinetic conditions were obtained by recycling the outlet gas mixture with a recycling ratio of ~180. This high speed of recirculation induced a slight pressure increase of ~0.2 atm.

The reactants and products were analyzed with a HP5890 Series II chromatograph. Prior to the detection and quantification on a catharometer, CO, CO_2, N_2, and N_2O were separated on two concentric columns (CTR1) from Alltech held at 30°C. CO and N_2 were separated on the inner column packed with a molecular sieve 0.5 nm, while N_2O and CO_2 were separated on the outer one packed with Porapack Q.

The specific rates of reactions were calculated according to

$$r_i = \frac{D_i \tau_i}{m}, \qquad [1]$$

where D_i was the N_2O or CO flow rate (mol h^{-1}), m was the mass of catalyst, and τ_i was the initial conversion ($i =$ N_2O or CO) calculated by extrapolating the deactivation curves at $t = 0$ according to the procedure earlier described in Ref. (18).

3. RESULTS

Steady-state activity measurements were performed under differential conditions at atmospheric pressure and various temperatures between 260 and 320°C. Two sets of experiments were performed by varying the partial pressure of N_2O and CO at constant P_{CO} and P_{N_2O} respectively. Figures 1 and 2 illustrate the influence of the partial

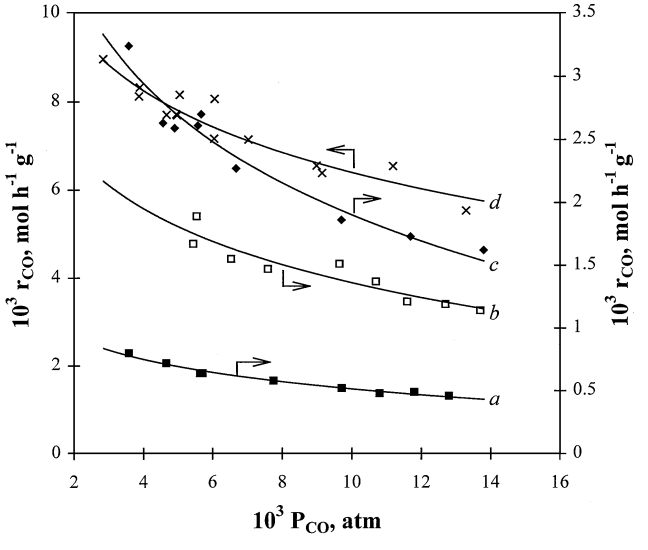

FIG. 1. Influence of the partial pressure of CO on the rate of the $CO + N_2O$ reaction on Pt/Al_2O_3 at various temperatures: a, 260°C; b, 280°C; c, 300°C; d, 320°C.

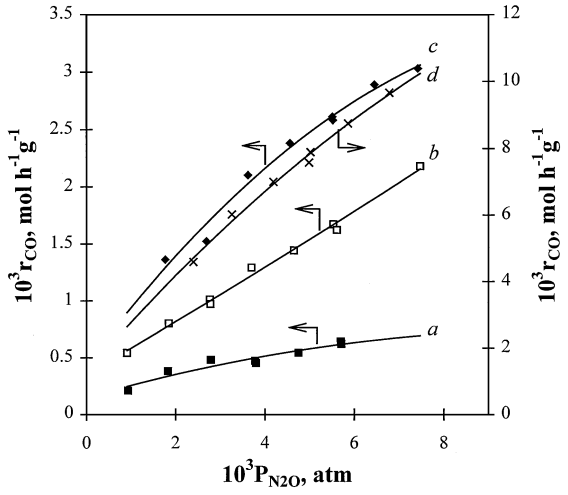

FIG. 2. Influence of the partial pressure of N_2O on the rate of the CO + N_2O reaction on Pt/Al_2O_3 at various temperatures: a, 260°C; b, 280°C; c, 300°C; d, 320°C.

pressures of the reactants on the rate. Let us note that the rate of the CO + N_2O reaction, at 300°C under stoichiometric conditions ($P_{CO} = P_{N_2O} = 5.6 \times 10^{-3}$ atm), is about one order of magnitude higher than that of the CO + NO reaction on 1 wt% Pt/Al_2O_3 (2.6×10^{-3} against 2.3×10^{-4} mol h^{-1} g^{-1}) with $P_{CO} = P_{NO} = 5 \times 10^{-3}$ atm and $T = 300$°C (16). It should be noted that different batches of Pt/Al_2O_3 were used to study these two reactions, although both samples were prepared by the same procedure. Nevertheless, the change in activity of a factor 10 cannot be accounted for by changes in the metal dispersion which was respectively 0.55 (16) and 0.58. Finally let us mention that our results differ from those of Adlhoch *et al.* (10) on a Pt polycrystalline catalyst and Mac Cabe and Wong (9) on Rh/Al_2O_3 who observed the reverse trend, i.e., that Pt and Rh are more active in the CO + NO reaction than in the CO + N_2O reaction.

The apparent orders have been calculated using linear regression analysis; they are reported in Table 1. Negative orders with respect to P_{CO} and positive values with respect to P_{N_2O} are obtained on Pt/Al_2O_3.

TABLE 1

Temperature Dependence on the Kinetic Parameters for the CO + N_2O Reaction on Pt/Al_2O_3

Temp. (°C)	$10^3 \times P_{N_2O}$ (atm)	$10^3 \times P_{CO}$ (atm)	m^a	n^a
320	2.4–6.8	2.9–13.3	−0.34	0.66
300	1.8–7.4	3.6–13.8	−0.51	0.60
280	0.9–7.5	5.4–13.7	−0.55	0.66
260	0.9–5.8	3.6–12.8	−0.43	0.65

[a] Rate, $r_{CO} = k \times P_{CO}^m \times P_{N_2O}^n$.

4. DISCUSSION

Let us first check whether the kinetic measurements are made under chemical control measurements. Taking into account the very high recirculation rate, external transfer limitations are not likely to occur. Nevertheless, it has been checked that using the same space velocity but with different amounts of catalysts, the conversion is approximately constant. But intragranular mass or heat transfer limitations could take place. By assuming a Knudsen diffusion regime, the efficient diffusion coefficient for N_2O is calculated to be about 10^{-6} m^2 s^{-1}. With a value of k of 4.4×10^{-2} mol h^{-1} g^{-1} and energy of activation of 134 kJ mol^{-1} as measured from the kinetic measurements, the effectiveness factor η is, respectively, 0.999, 0.99, and 0.94 at 327, 377, and 427°C, that is in the temperature range of this study. Hence internal mass transfer restrictions will not limit the measurements.

Concerning heat transfer limitations, the value of β_1 (the Prater number) (19) is between 2×10^{-4} and 3.4×10^{-4} which corresponds to ΔT_{max} (between the grain and its surface) less than 0.2°C. In conclusion the results reported here are under chemical control.

4.1. Surface Reaction Modeling

Up to now several mechanisms have been proposed after either transient or steady-state kinetic investigations and mathematical models have been consecutively derived to explain complex kinetic phenomena such as the dynamic behavior and the steady-state multiplicity behavior of the CO + N_2O reaction (20, 21). According to the literature it is often difficult to describe these different processes from a single mechanism. Some authors have suggested that these experimental observations could be related to changes in the rate-limiting step (20). Most of the mechanisms already proposed include reversible nondissociative adsorption of CO on metals (8, 9, 14). Concerning N_2O, its chemisorption on Pt has not been observed between 427 and 1327°C under UHV conditions (22) and numerous articles dealing with the kinetics of the CO + N_2O reaction have assumed dissociative adsorption of N_2O leading to chemisorbed O atoms and gaseous N_2. The production of CO_2 is assumed to mainly occur via a bimolecular reaction between CO_{ads} and O_{ads}. An alternative mechanism, earlier proposed by Takoudis *et al.* (23), involves the formation of adsorbed N_2O species on Pt polycrystalline before their decomposition between 400 and 1200°C. Such a mechanism has also been adopted by Mac Cabe and Wong (9) for the description of the kinetic behavior of Rh/Al_2O_3 in the CO + N_2O reaction. Finally a reaction between gaseous CO and adsorbed O atoms has also been considered as a possible route for the formation of CO_2 (24).

We have selected five mechanisms among those proposed in the literature that seemed the most plausible. As seen in Fig. 3, they mainly differ from each other by the step

Mechanism 1

[2] $CO + * \Leftrightarrow CO*$
[3] $N_2O + * \Leftrightarrow N_2O*$
[4] $N_2O* \rightarrow N_2 + O*$
[5] $CO* + O* \rightarrow CO_2 + 2*$

Mechanism 2

[2] $CO + * \Leftrightarrow CO*$
[3] $N_2O + * \Leftrightarrow N_2O*$
[6] $N_2O* + * \rightarrow N_2 + O* + *$
[5] $CO* + O* \rightarrow CO_2 + 2*$

Mechanism 3

[2] $CO + * \Leftrightarrow CO*$
[3] $N_2O + * \Leftrightarrow N_2O*$
[7] $N_2O* + CO* \rightarrow N_2 + CO_2 + 2*$

Mechanism 4

[2] $CO + * \Leftrightarrow CO*$
[8] $N_2O + * \rightarrow N_2 + O*$
[5] $CO* + O* \rightarrow CO_2 + 2*$

Mechanism 5

[2] $CO + * \Leftrightarrow CO*$
[9] $N_2O + CO* \rightarrow N_2 + CO_2 + *$

FIG. 3. Selected mechanisms for the $CO + N_2O$ reaction over noble metals.

of N_2O decomposition which is usually considered as rate determining. We have also considered the possibility that a vacant Pt site would be required for the dissociation of N_2O_{ads} in step [6]. This was suggested by previous surface science studies (25, 26) which showed that space and geometric considerations are crucial for the chemisorption of N_2O and its subsequent dissociation into gaseous N_2 and O_{ads}.

We have not considered that the bimolecular reaction $CO_{ads} + O_{ads}$ (step [5]) could be rate controlling based on results either reported in the literature (9) or obtained in our laboratory in a previous investigation of the $CO + NO + O_2$ reactions over noble metals (27). Indeed, it has been shown that the rate of the $CO + O_2$ reaction is much faster than the $CO + NO$ reaction on Pt/Al_2O_3, this last reaction taking place only when oxygen in the feed is almost completely consumed, showing that the reaction $CO_{ads} + O_{ads}$ is not rate limiting but that it is very fast. Since the $CO + N_2O$ is also slower than the $CO + O_2$ reaction (light-off temperature of ~330°C, against 290°C), the step $CO_{ads} + O_{ads}$ is not likely to be rate limiting. Moreover, the fact that the decomposition of N_2O is very slow on Pt/Al_2O_3 (conversion of only ~6% at 500°C) and that CO addition sharply increases the conversion of N_2O is an additional argument in favor of a fast step for CO oxidation.

A similar procedure, described in Ref. (16), has been used to derive a rate expression from each mechanism selected in this paper based on the following assumptions: (i) fast and competitive adsorptions of the reactants on Pt and (ii) CO and N_2O are the most abundant species at the surface. Since step [5] is likely to be very fast, as discussed above, adsorbed oxygen atoms are very reactive and, consequently, the oxygen coverage can be considered as negligible.

According to these assumptions, the following equations were obtained:

$$\text{mechanism 1} \quad r_{CO} = k_4\,\theta_{N_2O} \qquad [10]$$

$$\text{mechanism 2} \quad r_{CO} = k_6\,\theta_{N_2O}\theta_V \qquad [11]$$

$$\text{mechanism 3} \quad r_{CO} = k_7\,\theta_{N_2O}\theta_{CO} \qquad [12]$$

$$\text{mechanism 4} \quad r_{CO} = k_8\,P_{N_2O}\theta_V \qquad [13]$$

$$\text{mechanism 5} \quad r_{CO} = k_9 P_{N_2O}\theta_{CO}. \qquad [14]$$

θ_i and θ_v are respectively the surface coverage for compound i ($i = CO$ or N_2O) and the fraction of vacant sites at the surface. Equations [10] to [14] can be expressed as a function of unknown parameters, λ_{N_2O} and λ_{CO}, the adsorption equilibrium constants of N_2O and CO, and k_n, the rate constant of the limiting step, and of the partial pressures of the reactants according to Eqs. [15] to [19] in Table 2. Equations [20] to [24] correspond to their linearized expressions.

TABLE 2

Rate Expressions for the $CO + N_2O$ Reaction Derived from Mechanisms 1 to 5

Mechanism	RDS	Rate		Linearized expression of the rate	
1	$N_2O* \xrightarrow{k_4}$	$r_{CO} = \frac{k_4\lambda_{N_2O}P_{N_2O}}{1+\lambda_{CO}P_{CO}+\lambda_{N_2O}P_{N_2O}}$	[15]	$\frac{P_{N_2O}}{r_{CO}} = \frac{1+\lambda_{CO}P_{CO}+\lambda_{N_2O}P_{N_2O}}{k_4\lambda_{N_2O}}$	[20]
2	$N_2O* + * \xrightarrow{k_6}$	$r_{CO} = \frac{k_6\lambda_{N_2O}P_{N_2O}}{\left(1+\lambda_{CO}P_{CO}+\lambda_{N_2O}P_{N_2O}\right)^2}$	[16]	$\sqrt{\frac{P_{N_2O}}{r_{CO}}} = \frac{1+\lambda_{N_2O}P_{N_2O}+\lambda_{CO}P_{CO}}{\sqrt{k_6\lambda_{N_2O}}}$	[21]
3	$N_2O* + CO* \xrightarrow{k_7}$	$r_{CO} = \frac{k_7\lambda_{CO}\lambda_{N_2O}P_{N_2O}P_{CO}}{\left(1+\lambda_{CO}P_{CO}+\lambda_{N_2O}P_{N_2O}\right)^2}$	[17]	$\sqrt{\frac{P_{N_2O}P_{CO}}{r_{CO}}} = \frac{1+\lambda_{N_2O}P_{N_2O}+\lambda_{CO}P_{CO}}{\sqrt{k_7\lambda_{CO}\lambda_{N_2O}}}$	[22]
4	$N_2O + * \xrightarrow{k_8}$	$r_{CO} = \frac{k_8 P_{N_2O}}{1+\lambda_{CO}P_{CO}}$	[18]	$\frac{P_{N_2O}}{r_{CO}} = \frac{1+\lambda_{CO}P_{CO}}{k_8}$	[23]
5	$N_2O + CO* \xrightarrow{k_9}$	$r_{CO} = \frac{k_9\lambda_{CO}P_{N_2O}P_{CO}}{1+\lambda_{CO}P_{CO}}$	[19]	$\frac{P_{CO}P_{N_2O}}{r_{CO}} = \frac{1+\lambda_{CO}P_{CO}}{k_9\lambda_{CO}}$	[24]

4.2. Discrimination of a Mechanism for the $CO + N_2O$ Reaction on Pt/Al_2O_3 at 300°C

Clearly Eq. [19] is unable to model the CO partial pressure dependency of the rate since it is not compatible with a negative order in CO. Also Eq. [18] does not fit with the apparent N_2O orders which noticeably differ from 1 (see Table 1). Consequently mechanisms 4 and 5 can be discarded.

The discrimination between the three other mechanisms has been achieved using the graphic method previously detailed in Ref. (16). Although the linear plots obtained for P_{N_2O}/r_{CO}, $\sqrt{P_{N_2O}/r_{CO}}$, and $\sqrt{P_{N_2O}P_{CO}/r_{CO}}$ vs P_{CO} and P_{N_2O} do not allow the correct mechanism to be selected, this discrimination can be obtained from the examination of k_n, λ_{N_2O}, and λ_{CO}, calculated from the intercepts (β_{CO} and β_{N_2O}) and the slopes (α_{CO} and α_{N_2O}) of the straight lines. As a matter of fact in each case, we have four equations to calculate only three parameters. Hence k_n, λ_{N_2O}, and λ_{CO} can be calculated by several ways by using different sets of three equations. The comparison between the values of k_n, λ_{N_2O}, and λ_{CO} calculated in different ways can be a means to validate the value of the parameters. We have calculated two sets of values for the three parameters using respectively α_{CO}, α_{N_2O}, and β_{CO} and α_{CO}, α_{N_2O}, and β_{N_2O}. The results for Eqs. [15]–[17] are reported in Table 3.

It is clear that, while the set of equations based on α_{CO}, α_{N_2O}, and β_{CO} lead to positive and reasonable values for k_n, λ_{N_2O}, and λ_{CO}, α_{CO}, α_{N_2O}, and β_{N_2O} lead to negative values for λ_{N_2O} and λ_{CO} in Eqs. [15] and [17]. On the contrary, the two sets of values of k_n, λ_{N_2O}, and λ_{CO} in Eq. [16] are close to each other. Moreover, the value of λ_{CO} obtained from Eq. [16] is of the same order of magnitude as that calculated from the results of the kinetics of the CO + NO reaction on a similar Pt/Al_2O_3 catalyst ($\lambda_{CO} = 121$ atm^{-1}). Consequently, on the basis of this analysis, Eq. [16] derived from mechanism 2 seems to be preferred.

The calculation of k_n, λ_{N_2O}, and λ_{CO} has also been carried out by an optimization method (16) using the solver on Excel 5 from Microsoft. The adjustment of the unknown parameters is obtained when γ, the residual sum of squares between the experimental and calculated rates, using Eqs. [15] to [19], tends towards the lowest value.

$$\gamma = \sum_{i=1}^{n} (r_{i,\text{exp}} - r_{i,\text{calc}})^2. \qquad [25]$$

The lowest value for γ is obtained by comparing experimental and calculated rates using Eq. [16]. It is also observable that only Eq. [16] leads to a reasonable agreement between the adjusted parameters and those obtained from the graphic method. Accordingly, both observations show that only Eq. [16], derived from mechanism 2, can satisfactorily model the partial pressure dependencies of the rate at 300°C.

Let us now comment on the difference between the two values of λ_{CO} (78 and 121 atm^{-1}) obtained respectively in the CO + N_2O and CO + NO reactions at 300°C (Table 4). First, it must be noticed that, as mentioned above, the order of magnitude is the same, and the two values could simply be within the margin of error which is rather high considering the uncertainties on the rate measurements (mainly due to the extrapolation). But, there could also be some physical reasons for the observed difference. First, it should also be kept in mind that they have been obtained on different Pt catalysts. But they were prepared according to the same procedure, and their dispersion slightly differs; consequently it is not reasonable to assume that they

TABLE 3

Kinetic and Thermodynamic Adsorption Constants for the CO + N_2O Reaction over Pt/Al_2O_3 at 300°C

Mechanism	Rate Eq.	α_i[a] i = CO	α_i[a] i = N_2O	β_i[b] i = CO	β_i[b] i = N_2O		λ_{CO} (atm^{-1})	λ_{N_2O} (atm^{-1})	k_n (mol g^{-1} cat h^{-1})
1	[15]	179.2	200.1	1.211	0.983	[c]	2.6×10^3	2.9×10^3	5.0×10^{-3}
						[d]	-3.2×10^3	-3.6×10^3	5.0×10^{-3}
						[e]	1.6×10^4	1.7×10^3	5.10×10^{-3}
2	[16]	45.7	55.3	0.978	0.898	[c]	69	83	2.73×10^{-2}
						[d]	72	87	2.85×10^{-2}
						[e]	78	90	2.80×10^{-2}
3	[17]	14.0	5.1	0.033	0.079	[c]	3.6×10^3	1.3×10^3	1.40×10^{-2}
						[d]	-1.7×10^{-1}	-6.3×10^{-2}	1.40×10^{-2}
						[e]	2.0×10^7	7.0×10^6	1.30×10^{-2}

[a] Slopes of the linear plots $\sqrt{P_{N_2O}P_{CO}/r_{CO}}$, $\sqrt{P_{N_2O}/r_{CO}}$, and P_{N_2O}/r_{CO} vs P_{N_2O} and P_{CO}.
[b] Intercepts of the linear plots $\sqrt{P_{N_2O}P_{CO}/r_{CO}}$, $\sqrt{P_{N_2O}/r_{CO}}$, and P_{N_2O}/r_{CO} vs P_{N_2O} and P_{CO}.
[c] Using α_{CO}, α_{N_2O}, β_{CO}.
[d] Using α_{CO}, α_{N_2O}, and β_{N_2O}.
[e] From the optimization method.

TABLE 4

Comparison of the Kinetic Data Obtained at 300°C on Pt/Al_2O_3 for the CO + NO and CO + N_2O Reactions

Reaction	$10^3 P_{CO}$ (atm)	10^3 (P_{NO} or P_{N_2O}) (atm)	λ_{NO} or λ_{N_2O} (atm^{-1})	λ_{CO} (atm^{-1})	k_n[a] (mol h^{-1} g^{-1})
CO + NO	5–9	1.5–5.6	11	121	1.14×10^{-2}
CO + N_2O	3.6–13.8	1.8–7.4	90	78	2.80×10^{-2}

[a] Rate constant for the dissociation step of N_2O ($N_2O^* + * \rightarrow N_2 + O^* + *$), and of NO ($NO^* + * \rightarrow N^* + O^*$).

could have different adsorptive properties. The accumulation of various intermediate species during the CO + NO and CO + N_2O reactions could also modify the adsorptive properties of Pt. For instance Lorimer and Bell (6) have suggested that the formation of isocyanate species on the support during the CO + NO reaction could deactivate the neighboring Pt atoms by electronic modifications. Additionally, the different buildup of chemisorbed O atoms from the dissociation of N_2O and NO could alter differently the electronic properties of Pt surface atoms. According to the model of description for transition metals and CO bond, proposed earlier by Blyholder (28), the higher electronegativity of oxygen could induce a decrease in the electron density of Pt atoms located at the vicinity of chemisorbed O atoms. Accordingly the extent of electron back-donation would decrease further weakening the metal–CO bond.

Now, one can discuss on the validity of the selected mechanism. Presently, among the mechanisms already suggested in the literature, most of them assumed the dissociation of N_2O as the rate-determining step. Nevertheless, only a few of them associate a nearest neighbor vacant site to dissociate N_2O molecules adsorbed on metals. To our knowledge only Permana *et al.* (29) have recently kept in consideration this hypothesis on Rh. This suggestion can be argued in light of previous studies which have shown that the extent of N_2O dissociation depends on the surface atom arrangement. For instance Li and Bowker (26) have found a clear structural dependence of nitrous oxide adsorption and decomposition on Rh (111) and Rh (110). Recently, calculations using an extended Huckel method have been performed in our laboratory to identify the most stable geometrical configuration of N_2O adsorbed on a Pt cluster. Among the configurations considered, the lowest energy of adsorption was obtained when N_2O is upright with the terminal N atom bonded to a Pt atom. Such findings suggest that Pt atoms at the vicinity of adsorbed N_2O should be involved in the N–O bond breaking leading to O adsorbed on a second Pt adsorption site. Hence, our observations are in line with the conclusions drawn from these earlier investigations supporting the occurrence of dissociation of adsorbed N_2O on a free adjacent Pt site.

Let us now compare the value of k and λ_{N_2O} for the CO + N_2O reaction with those of k and λ_{NO} previously obtained for the CO + NO reaction on Pt/Al_2O_3 (16) (Table 4). As shown before, Pt/Al_2O_3 is more active in the CO + N_2O reaction than in the CO + NO reaction which contradicts previous observations reported by Adlhoch *et al.* on Pt (10) who found the reverse trend. The results reported by Adlhoch *et al.* could be explained on the basis of Cho's statements (14) developed in the introduction, the lowest activity of Pt could be related to the highest value of λ_{CO} in the CO + N_2O reaction in comparison with the CO + NO reaction. In this study no significant modification in the CO-inhibiting effect could explain the large difference in the activity of Pt/Al_2O_3 for both reactions. On the other hand λ_{N_2O} is six times higher than λ_{NO}. Such a difference indicates that N_2O adsorbs on Pt/Al_2O_3 more strongly than NO. This result seems consistent with a previous investigation of the decomposition of NO and N_2O on Pt wire (23). The authors have found respectively −89 and −34.5 kJ mol^{-1} for the adsorption enthalpies of N_2O and NO. It is also noticeable that the rate constants of NO and N_2O dissociation vary in the same order as λ_i. Such a correlation can easily be explained from the current description model used for modeling the adsorption and dissociation of N_2O which involves a back-donation of *d* electrons of metal into the antibonding orbital of N_2O. This charge transfer would strengthen the Pt–N bond and subsequently weaken the terminal N–O bond further facilitating the N–O bond breaking. To summarize, the higher activity of Pt for the CO + N_2O compared with the CO + NO reaction is attributable to a stronger adsorption of N_2O and higher reactivity of adsorbed N_2O compared with NO, rather than a decrease in the inhibiting effect of CO since λ_{CO} does not change significantly.

To illustrate this conclusion one can examine the temperature-programmed conversion curves for the CO + NO and CO + N_2O reaction on Pt/Al_2O_3 in Fig. 4. The continuous decrease in the selectivity for the formation of N_2O, S_{N_2O}, at low temperature and low NO conversion, can be explained by the competitive adsorptions of N_2O and NO in favor of N_2O which can subsequently react with CO even better since the dissociation rate constant of N_2O is higher than that of NO. As a matter of fact, S_{N_2O} in the CO + NO reaction is influenced by several factors. It is well known that the reduction of NO by CO is a complex system

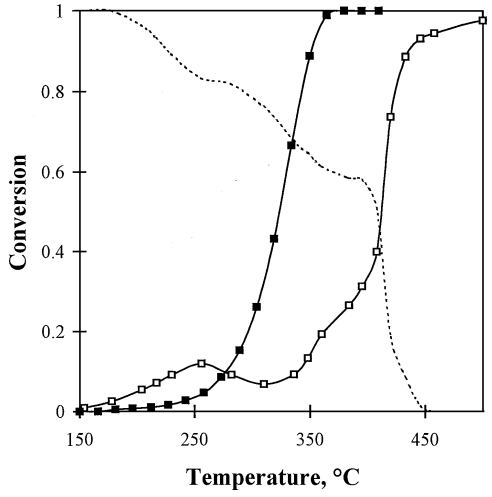

FIG. 4. Comparative temperature-programmed experiments of the CO + N_2O and CO + NO reactions on Pt/Al_2O_3 under stoichiometric conditions ($P^0_{N_2O} = P^0_{CO} = 6 \times 10^{-3}$ atm for the CO + N_2O reaction; $P^0_{NO} = P^0_{CO} = 5 \times 10^{-3}$ atm for the CO + NO reaction; space velocity 25,000 h^{-1}). . . . , N_2O selectivity in the CO + NO reaction; ■, conversion of CO by reaction with N_2O; □, conversion of CO by reaction with NO.

of competitive–successive reactions:

$$2CO + 2NO \rightarrow N_2 + 2CO_2 \quad [26]$$

$$CO + 2NO \rightarrow N_2O + CO_2 \quad [27]$$

$$CO + N_2O \rightarrow N_2 + CO_2. \quad [28]$$

Hence S_{N_2O} is affected by the relative rates of reactions [26], [27], and [28] and consequently by the initial selectivity of NO conversion (into N_2 and N_2O) and by the secondary reaction [28] which are themselves both influenced by temperature and the conversion of NO. The rates of NO and N_2O conversions in the system CO + NO can be expressed as

$$r_{N_2O} = \frac{k_{N_2O}\lambda_{N_2O}P_{N_2O}}{\left(1 + \lambda_{N_2O}P_{N_2O} + \lambda_{NO}P_{NO} + \lambda_{CO}P_{CO}\right)^2} \quad [29]$$

$$r_{NO} = \frac{k_{NO}\lambda_{NO}P_{NO}}{\left(1 + \lambda_{N_2O}P_{N_2O} + \lambda_{NO}P_{NO} + \lambda_{CO}P_{CO}\right)^2} \quad [30]$$

according to this study and previous results on the kinetics of NO reduction by CO (16). Equation [29] shows that, at a given temperature, when CO and NO conversion increase, r_{N_2O} (and N_2O conversion) increases. It is more difficult to discuss on the changes of r_{NO} since while the order in NO is positive on Pt (0.95 at 300°C), that in CO is negative (−0.84 at 300°C) (16), but it is clear that the ratio $(r_{N_2O}/r_{NO}) = (k_{N_2O}\lambda_{N_2O}P_{N_2O}/k_{NO}\lambda_{NO}P_{NO})$ increases as NO conversion increases.

These observations can qualitatively explain the changes of S_{N_2O} in Fig. 4 for the CO + NO reaction. Of course, as previously mentioned, the influence of temperature on CO, NO, and N_2O adsorption and on the rate constants should be taken into account in addition to the influence of the conversion.

4.3. *Influence of Temperature*

Estimation of the adsorption enthalpies of the reactants and of the activation energy of the dissociation step of adsorbed N_2O. If Eq. [16] is to be used to model the functioning of a TWC under actual conditions, it must be modified to include the effect of temperature, T.

$$r_{CO} = \frac{A\exp\left[-\frac{E}{RT}\right] f_{N_2O}\exp\left[-\frac{\Delta H_{ads,N_2O}}{RT}\right]P_{N_2O}}{\left(1 + f_{N_2O}\exp\left[-\frac{\Delta H_{ads,N_2O}}{RT}\right]P_{N_2O} + f_{CO}\exp\left[-\frac{\Delta H_{ads,CO}}{RT}\right]P_{CO}\right)^2}. \quad [31]$$

Equation [31] so obtained includes unknown parameters such as A and f_i, the preexponential factors; E, the energy of activation of the rate-determining step; and $\Delta H_{ads,i}$ the adsorption enthalpy for compound i ($i = N_2O$ or CO). R is the ideal gas constant. The quantitative evaluation of these parameters has been achieved by additional kinetic measurements at various temperatures between 260 and 320°C (Figs. 1 and 2) with CO conversion ranging between 1.5 and 40%. The plots $\sqrt{P_{N_2O}/r_{CO}}$ vs P_{CO} and P_{N_2O} obtained from these kinetic data are linear which show that the rate equation remains valid in the temperature range considered. The results of the calculation of λ_i and k_6 using the graphic and the optimization methods are reported in Table 5.

TABLE 5

Effect of Temperature on the Kinetic and Thermodynamic Adsorption Constants for the CO + N_2O Reactions over Pt/Al_2O_3

	α_i[a]		β_i[a]				
Temp. (°C)	i = CO	$i = N_2O$	i = CO	$i = N_2O$	λ_{N_2O} (atm^{-1})	λ_{CO} (atm^{-1})	$k_6 \times 10^2$ (mol g^{-1} h^{-1})
260	93.6	184.2	2.09	1.74	154/142[b]	90/85[b]	0.48/0.57[b]
280	69.5	88.7	1.32	1.27	102/111[b]	84/81[b]	1.32/1.27[b]
320	21.3	33.6	0.69	0.62	65/53[b]	42/41[b]	5.80/6.40[b]

[a] Slope and intercept of the linear plots $\sqrt{P_{N_2O}/r_{CO}}$ vs P_{N_2O} and P_{CO}.
[b] From the optimization method.

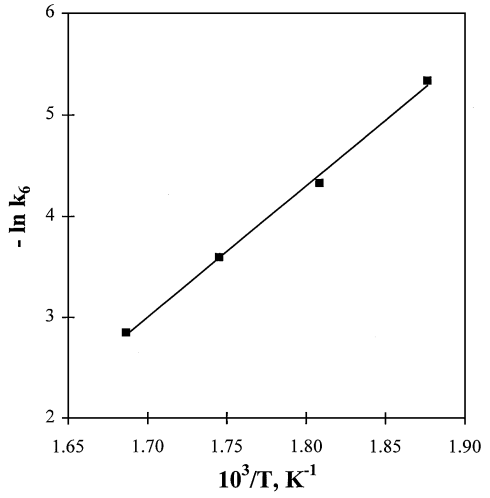

FIG. 5. Estimation of the activation energy of the dissociation step of adsorbed N_2O on Pt/Al_2O_3.

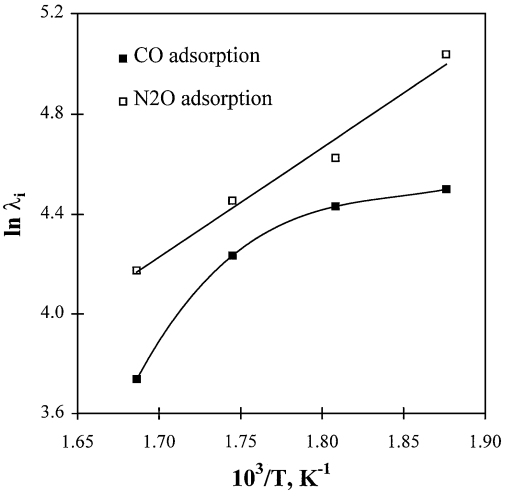

FIG. 6. Temperature dependency of the adsorption equilibrium constants of N_2O and CO on Pt/Al_2O_3 between 260 and 320°C.

From these parameters we have estimated A, f_i, $\Delta H_{\text{ads},i}$, and E.

Figures 5 and 6 show approximate linear plots respectively for $\ln k_6$ and $\ln \lambda_{N_2O}$ vs $1/T$ while the slope of the curve $\ln \lambda_{CO}$ vs $1/T$ seems to decrease when the temperature increases. This could be assigned to an adsorbate surface coverage dependency of the enthalpy of CO adsorption in the temperature range of this study, although this result must be considered with caution taking into account the large margin of error in the value of λ_i. Consequently, in a first approach we have considered constant values for the adsorption enthalpies in the range of temperature and of partial pressures of the reactants used in this study.

A and f_i (the preexponential factors), $\Delta H_{\text{ads},i}$, and E have been calculated respectively from the intercepts and the slopes of the straight lines in Figs. 5 and 6. According to our typical conditions, we have considered an average value of -29 kJ mol^{-1} for $\Delta H_{\text{ads,CO}}$. The corresponding values are reported in Table 6. They are compared with the set of values optimized with the solver. When using the solver the procedure is more complex than in the first part of this study since six parameters (E, $\Delta H_{\text{ads,CO}}$, $\Delta H_{\text{ads},N_2O}$, A, f_{CO}, f_{N_2O}) are included in the calculation model (Eq. [31]) instead of three in Eq. [16]. A quadratic extrapolation has been preferred for adjusting the parameters since they cannot be separated. The linear plot of the calculated rates as a function of the experimental ones in Fig. 7 with a slope close to 1 shows that the proposed kinetic model approximately fits our kinetic measurements between 260 and 320°C. Additionally the optimized values in Table 6 are comparable with those obtained from the graphic method.

Validity of the kinetic model in temperature-programmed experiments. In order to check the validity of the rate expression we have performed a temperature-programmed experiment on 0.2 g of Pt/Al_2O_3 reduced *in situ* in flowing hydrogen at 500°C and outgassed in flowing N_2 at 400°C to remove chemisorbed hydrogen. The reaction was studied under stoichiometric conditions with initial partial pressures $P^0_{N_2O} = P^0_{CO}$ of 6×10^{-3} atm, hence with $\tau_{N_2O} = \tau_{CO}$. Then using the expression

TABLE 6

Preexponential Factors, Heat of N_2O and CO Adsorption, and Activation Energy for the Dissociation of Adsorbed N_2O on Pt/Al_2O_3

Method	Preexponential factors			Heat of adsorption, kJ mol^{-1}		
	A^b	f_{CO}, atm^{-1}	f_{N_2O}, atm^{-1}	$-\Delta H_{\text{ads},N_2O}$	$-\Delta H_{\text{ads,CO}}$	E^a, kJ mol^{-1}
[c]	1.9×10^8	9.0×10^{-2}	4.1×10^{-2}	36.5	29	108
[d]	4.4×10^8	12.0×10^{-2}	5.2×10^{-2}	34.3	28.6	112

[a] Energy of activation for the reaction step ($N_2O^* + * \rightarrow N_2 + O^* + *$).
[b] mol h^{-1} g^{-1} cat.
[c] From the graphic plots $\ln \lambda_i$, $\ln k$ vs $1/T$.
[d] From the optimization method.

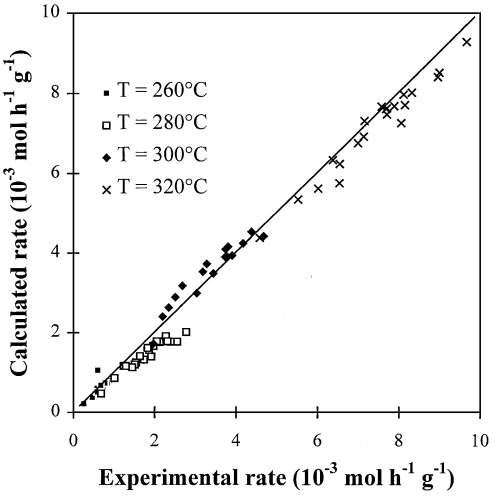

FIG. 7. Correlation between experimental and calculated rates from Eq. [31].

$$r_{CO} = \frac{D_{CO}\tau_{CO}}{m} = \frac{k_6\lambda_{N_2O}(1-\tau_{N_2O})P^0_{N_2O}}{\left[1+\lambda_{N_2O}(1-\tau_{N_2O})P^0_{N_2O}+\lambda_{CO}(1-\tau_{CO})P^0_{CO}\right]^2}, \quad [32]$$

with $D_{CO} = 2.46 \times 10^{-3}\,\text{mol}\,h^{-1}$, taking into account the temperature dependency of k_6, λ_{CO}, and λ_{N_2O}, τ_{CO} can be calculated. The calculation of τ_{CO} at various temperature was achieved using the optimised values of E, $\Delta H_{ads,CO}$, $\Delta H_{ads,N_2O}$, and the preexponential factors f_{CO}, f_{N_2O}, and A in Table 6. Hence the equation to be solved was

$$1.23 \times 10^{-2}\tau_{CO} = \frac{1.38 \times 10^5 \exp\left(-\frac{9350}{T}\right)(1-\tau_{CO})}{\left[1+3.12 \times 10^{-4}\exp\left(\frac{4100}{T}\right)(1-\tau_{CO})+7.2 \times 10^{-4}\exp\left(\frac{3420}{T}\right)(1-\tau_{CO})\right]^2}. \quad [33]$$

Figure 8 shows the comparison between the predicted and experimental CO conversion curves versus temperature. The fit between the two curves is not good, particularly at temperatures above 335°C.

Such a discrepancy could originate from (i) an invalid kinetic model, (ii) heat transfer limitations, and (iii) changes in the adsorption enthalpies with surface coverages.

As mentioned at the beginning of the discussion, heat transfer is not likely to disturb our kinetic measurements. On the contrary, numerous investigations showed modifications in the strength of the CO–metal bond as a function of surface CO coverage (30–32). Moreover we have also observed by direct adsorption measurements of CO on Pt–Rh/Al_2O_3 that $\Delta H_{ads,CO}$ is surface coverage dependent (as a matter of fact $\Delta H_{ads,CO}$ seems to be a linear function of $\ln P_{CO}$) (33). Hence, we have attempted to quantify the dependency of $\Delta H_{ads,N_2O}$ and $\Delta H_{ads,CO}$ in the temperature range of the TP experiment in Fig. 8.

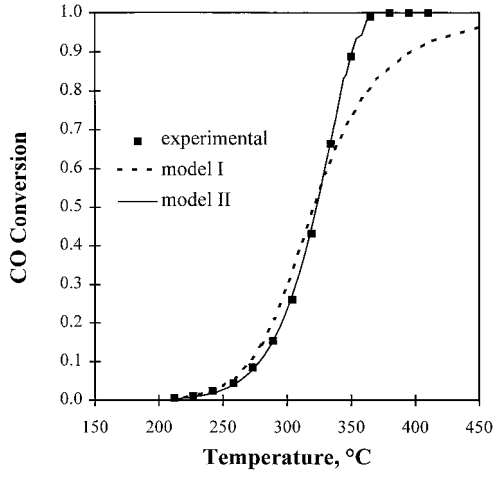

FIG. 8. Comparison between the experimental and predicted CO conversion curves vs. temperature on Pt/Al_2O_3 under stoichiometric conditions with $P^0_{N_2O} = P^0_{CO} = 6 \times 10^{-3}$ atm, $m = 0.2$ g of catalyst, and a space velocity of 25,000 h^{-1}. Model I is based on constant values for $\Delta H_{ads,i}$ in Table 6. Model II is based on changes in $\Delta H_{ads,i}$ with P_i (see Table 7).

In a first approach, we have considered only the changes of $\Delta H_{ads,N_2O}$ which will have more influence on the rate than $\Delta H_{ads,CO}$, $\lambda_{CO}P_{CO}$ being only at the denominator of Eq. [32] and always smaller than 1. These changes have been roughly approximated by neglecting the changes of the denominator of Eq. [32] with the partial pressure, hence the ratio between experimental and calculated CO conversion according to Eq. [32], $\tau_{CO,exp}/\tau_{CO,calc} \cong \lambda_{N_2O,exp}/\lambda_{N_2O,calc}$. This allows us to roughly estimate $\Delta H'_{ads,N_2O}$, the actual values of the enthalpy of N_2O adsorption, at various conversions (and partial pressures). As shown in Fig. 9 $\Delta H'_{ads,N_2O}$ vs

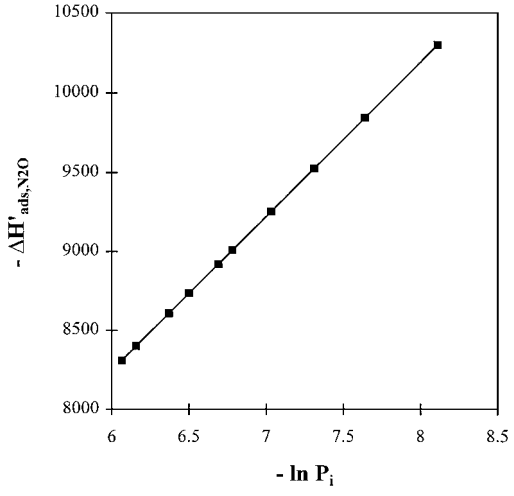

FIG. 9. Changes in the heat of N_2O adsorption on Pt/Al_2O_3 with the partial pressure P_i in the temperature range of the TP experiment performed under stoichiometric conditions, $P_i = P_{N_2O} = P_{CO}$.

TABLE 7

Influence of the Partial Pressures of the Reactants on the Adsorption Enthalpies of CO and N_2O over Pt/Al_2O_3

	f_i[a], atm^{-1}	a_i[b], kJ mol^{-1}	b_i[b], kJ mol^{-1}
N_2O adsorption	0.064	−12.2	3.9
CO adsorption	0.18	−2.8	5.0

[a] $\lambda_i = f_i \exp(-\Delta H_{ads,i}/RT)$, atm^{-1}.
[b] $\Delta H_{ads,i} = a_i + b_i \ln P_i$, kJ mol^{-1}.

P_i ($P_i = P_{N_2O} = P_{CO}$ under stoichiometric conditions) obeys a semilogarithmic relationship. Accordingly $\Delta H'_{ads,N_2O}$ can be described by

$$\Delta H'_{ads,N_2O} = a_{N_2O} + b_{N_2O} \ln P_i (\text{kJ mol}^{-1}), \qquad [34]$$

with $a_{N_2O} = -10.5$ kJ mol^{-1} and $b_{N_2O} = 4$ kJ mol^{-1}. Such an empirical equation has also been assumed for changes of $\Delta H_{ads,CO}$ vs the partial pressures.

$$\Delta H_{ads,CO} = a_{CO} + b_{CO} \ln P_i. \qquad [35]$$

Equations [34] and [35] have been substituted in Eq. [31]. Then the parameters f_i, a_i, and b_i have been adjusted by minimizing the square difference between $\tau_{CO,exp}$ and $\tau_{CO,calc}$ using the solver. The value of the preexponential A and of the activation energy E used for the calculation were similar to those reported in Table 6. The comparison between $\tau_{CO,exp}$ and $\tau_{CO,calc}$ in Fig. 8 shows a good quality of fit. The optimized values for f_i, a_i, and b_i are reported in Table 7. Let us note that we have neglected the temperature dependency of the adsorption enthalpies in the temperature range of the temperature-programmed experiment. This is a common simplification. Consequently the rate equation [31] accounts for experimental results obtained at various partial pressures of N_2O and CO and at various temperatures provided that the adsorption enthalpies changes vs surface coverage are taken into account.

Presently the modifications in the strength of the Pt–adsorbate bond with the surface coverage is not well understood. It could be related to either lateral repulsive interactions between molecules in the adsorption layer at saturation coverage or by a deactivation-induced effect on the electronic properties of Pt. Now it must be mentioned that these surface coverage dependencies of the adsorption enthalpies and consequently of the equilibrium adsorption constant λ_i do not invalidate the parameters values in Tables 3–5 that have been obtained by considering that λ_i is constant at a given temperature. The values reported for λ_i in these tables must be taken as average values valid in the rather narrow range of θ_i corresponding to the experimental conditions (for example, at 300°C the range of variation was between about 0.25 and 0.5 for θ_{CO} and 0.1 to 0.3 for θ_{N_2O}).

Finally, it should be stressed that Eqs. [34] and [35] were used for a stoichiometric mixture ($P_{CO} = P_{N_2O}$), for other compositions generalized equations should be used such as

$$\Delta H_{ads,N_2O} = a_{N_2O} + c_{N_2O} \ln P_{N_2O} + d_{N_2O} \ln P_{CO} \qquad [36]$$

$$\Delta H_{ads,CO} = a_{CO} + c_{CO} \ln P_{N_2O} + d_{CO} \ln P_{CO}. \qquad [37]$$

5. CONCLUSION

The purpose of this study was to investigate the kinetics of the $CO + N_2O$ reaction on Pt/Al_2O_3 both to propose a mechanism and to derive a rate expression in order to model this reaction under the actual conditions of TWCs and to try to explain the changes in the selectivity for N_2O production (S_{N_2O}) in the $CO + NO$ reaction.

Among the mechanisms that have been considered in this study we have selected the one which involves the following steps:

$$CO + {}^* \Leftrightarrow CO^*$$

$$N_2O + {}^* \Leftrightarrow N_2O^*$$

$$N_2O^* + {}^* \rightarrow N_2 + {}^* + O^*$$

$$CO^* + O^* \rightarrow CO_2 + 2^*.$$

A rate expression has been derived assuming the following hypotheses: (i) fast and competitive adsorptions of the reactants; (ii) the dissociation of N_2O adsorbed on Pt as rate limiting; and (iii) N_2O and CO as the most abundant adsorbed species at the surface, the oxygen surface coverage being assumed as negligible because the high reactivity of adsorbed O atoms.

In a first approach, by linearizing the rate expression, the rate constant of N_2O dissociation k_6 and the adsorption equilibrium constants of the reactants (λ_{CO} and λ_{N_2O}) on Pt have been calculated using both graphic and optimization procedures. Their comparison with the kinetic and thermodynamic constants from an earlier kinetic study of the $CO + NO$ reaction allow us to explain the difference in activities of Pt/Al_2O_3 in both reactions. N_2O is more strongly adsorbed on Pt/Al_2O_3 than NO and reacts slightly more readily as shown by the highest value for the N_2O dissociation rate constant.

The temperature dependencies of E, λ_{N_2O}, and λ_{CO} have been estimated. Clearly the adsorption enthalpies of the reactants depend on the surface coverage. The quantification of such effect leads to the equation

$$r_{CO} = \frac{2.9 \times 10^7 \exp\left(\frac{-11990 - 466 \ln P_i}{T}\right) (1 - \tau_{N_2O})\ P^0_{N_2O}}{\left[1 + 6.4 \times 10^{-2} \exp\left(\frac{1460 - 466 \ln P_i}{T}\right) (1 - \tau_{N_2O})\ P^0_{N_2O} + 18 \times 10^{-2} \exp\left(\frac{340 - 600 \ln P_i}{T}\right) (1 - \tau_{CO})\ P^0_{CO}\right]^2}.$$

This equation correctly fits our temperature-programmed experiments on Pt/Al_2O_3 particularly at high conversion. However, it is worth noting that this empirical expression of the rate is strictly applicable to feed composition close to the stoichiometry.

ACKNOWLEDGMENT

This work was supported by the Region Nord-Pas-de-Calais through Contract L961-01aN°31.

REFERENCES

1. Shelef, M., and Graham, G. W., *Catal. Rev. Sci. Eng.* **36**, 433 (1994).
2. Taylor, K. C., *Catal. Rev. Sci. Eng.* **35**, 457 (1993).
3. Zhdanov, V. P., *J. Catal.* **162**, 147 (1996).
4. Cho, B. K., *J. Catal.* **162**, 149 (1996).
5. Hecker, W. C., and Bell, A. T., *J. Catal.* **84**, 200 (1983).
6. Lorimer, D., and Bell, A. T., *J. Catal.* **59**, 223 (1979).
7. Bauerle, G. L., Service, G. R., and Nobe, K., *Ind. Eng. Chem. Prod. Res. Dev.* **11**, 54 (1972).
8. Cho, B. K., Shanks, B. H., and Bailey, J. E., *J. Catal.* **115**, 486 (1989).
9. Mac Cabe, R. W., and Wong, C., *J. Catal.* **121**, 422 (1990).
10. Adlhoch, W., Kohler, R., and Linz, H. G., *Z. Phys. Chem. N. F.* **120**, 111 (1980).
11. Dubois, L. H., Hansma, P. K., and Somorjai, G. A., *J. Catal.* **65**, 318 (1980).
12. Oh, S. H., Fisher, G. B., Carpenter, J. E., and Goodman, D. W., *J. Catal.* **100**, 360 (1986).
13. Banse, B. A., Wickham, D. T., and Koel, B. E., *J. Catal.* **119**, 238 (1989).
14. Cho, B. K., *J. Catal.* **138**, 255 (1992).
15. Cho, B. K., *J. Catal.* **148**, 697 (1994).
16. Granger, P., Dathy, D., Lecomte, J. J., Leclercq, L., Prigent, M., Mabilon, G., and Leclercq, G., *J. Catal.* **173**, 304 (1998).
17. Granger, P., Lecomte, J. J., Dathy, C., Leclercq, L., and Leclercq, G., *J. Catal.* **175**, 194 (1998).
18. Leclercq, G., Leclercq, L., and Maurel, R., *J. Catal.* **44**, 68 (1976).
19. Trambouze, P., Van Landeghem, H., and Wauquier, J.-P., *in* "Les réacteurs chimiques, conception, calcul, mise en œuvre." Technip, Paris, 1984.
20. Sadhankar, R. R., Ye, J., and Lynch, D. T., *J. Catal.* **146**, 511 (1994).
21. Sadhankar, R. R., and Lynch, D. T., *J. Catal.* **149**, 278 (1994).
22. Schmidt, L. D., Hansenberg, D., Schwartz, S., and Papapolymerou, G. A., *in* "Catalyst Characterization Science-Surface and Solid State Chemistry" (M. L. Deviney and J. L. Gland, Eds.), ACS Symposium Series 288, p. 177. Am. Chem. Soc., Washington, DC, 1985.
23. Takoudis, C. G., and Schmidt, L. D., *J. Catal.* **80**, 274 (1983).
24. Lintz, H. G., *Surf. Sci.* **108**, L486 (1981).
25. Daniel, W. M., Kim, Y., Peebles, H. C., and White, J. M., *Surf. Sci.* **111**, 189 (1981).
26. Li, Y., and Bowker, M., *Surf. Sci.* **384**, 67 (1996).
27. Leclercq, G., Dathy, C., Mabilon, G., and Leclercq, L., *in* "Catalysis and Automotive Pollution Control II" (A. Crucq Ed.), p. 181. Elsevier, Amsterdam, 1985.
28. Blyholder, G., *J. Phys. Chem.* **68**, 2772 (1964).
29. Permana, H., Ng, K. Y. S., Peden, C. H. F., Schmieg, S. J., Lambert, D. K., and Belton, D. N., *J. Catal.* **164**, 194 (1996).
30. Voogt, E. H., Coulier, L., Gijzman, O. L. J., and Geus, G. E., *J. Catal.* **169**, 359 (1997).
31. Seebauer, E. G., Kong, A. C. F., and Schmidt, L. D., *Surf. Sci.* **176**, 134 (1986).
32. Ertl, G., Neuman, M., and Streit, K. M., *Surf. Sci.* **64**, 393 (1977).
33. Granger, P., Lecomte, J. J., Leclercq, L., and Leclercq, G., to be published.